Estimation of a eutectic composition of imidazolium chloride ionic liquids using video imaging and impedance methods

Atsuhi Ooki [1], Kazuhisa Azumi [*2]

1. Graduate School of Chemical Engineering and Science, Hokkaido University

2. Graduate School of Engineering, *ibid*.

Abstract

The eutectic temperature T_e and composition X_e of binary systems composed of three ionic liquids, 1-ethyl-3-methylimidazolium chloride ([C_2mim]Cl), 1-methyl-3-propylimidazolium chloride ([C_3mim]Cl), and 1-butyl-3-methylimidazolium chloride ([C_4mim]Cl), were estimated using a video imaging method, in which the formation of a liquid phase on solidified ionic liquids at a given composition stored in a vial was detected from time-lapse images taken during temperature scanning. The advantage of this method is that multiple samples (five samples in this study) could be measured simultaneously, whereas its disadvantage is a less accurate determination of the melting point compared with the conventional differential scanning calorimetry (DSC) method. The T_e and X_e of [C_2mim]Cl–[C_3mim]Cl, [C_2mim]Cl–[C_4mim]Cl, and [C_3mim]Cl–[C_4mim]Cl binary systems were roughly estimated. Furthermore, the T_e of the ternary system of the [C_2mim]Cl–[C_3mim]Cl–[C_4mim]Cl with limited compositions was estimated, which was lower than that of the binary systems. The transition of the electrochemical impedance of [C_2mim]Cl ionic liquids was also measured using two Pt wire electrodes as a function of temperature. The differential inversed resistance curve (dR^{-1}/dT)-T shows an obvious peak corresponding to the phase transition from a low conductive solid phase to a highly conductive liquid phase. This peak was comparable with the peak obtained in the DSC measurement.

Keywords

Melting point, Eutectic temperature, Eutectic composition, Video imaging, phase diagram, impedance

1. Introduction

Ionic liquids (I.L.) are useful salts in a liquid phase at room temperature due to their attractive properties such as low pressure, high chemical stability, high electric conductivity, wide potential window, and high solubility for metal ions. As a result, many I.L. applications have been explored, including battery, electrodeposition, plating, and electrorefining. For example, electroplating of less-noble metals such as Al and Ti and their alloys from I.L. bath has been a major subject in this field. 1-ethyl-3-methylimidazolium chloride ([C_2mim]Cl) is a typical I.L. widely used for electrochemical applications due to its high conductivity and low melting point (T_m) achieved by mixing metal chlorides such as $AlCl_3$. On the other hand, the T_m of [C_2mim]Cl is approximately 353 K (80°C), considerably higher than room temperature; thus, lowering T_m is desirable for the convenience of some room-temperature applications without heating [1]. Mixing I.L. has been performed to adjust their properties, including T_m [2,3]. The lowest T_m is obtained at the eutectic composition for binary systems, such as 1-ethyl-3-methylimidazolium hexafluorophosphate ([Emim][PF6])–1-ethyl-2-methylpyrazolium hexafluorophosphate ([empz][PF_6]) [1], [1,3-diMeIm][4,5-diNO_2-Im]–[1,3-diMeIm][4-NO_2-Tri] [4], and 1-ethyl-3-methylimidazolium chloride ([C_2mim]Cl)–1-butyl-3-methylimidazolium chloride ([C_4mim]Cl) [5], and other binary systems [6].

In this work, three I.L. shown in **Fig. 1** composed of cations with common backbone and alkyl side chain with different lengths and common chloride anion were chosen to investigate the effect of mixing I.L. on T_m because their properties depend on the length of their alkyl chain [7.8]. Among them, [C_2mim]Cl has the shortest methyl group and, thus, the highest charge density, resulting in the highest T_m, which is approximately 353 K (80°C). However, the T_m of 1-methyl-3-propylimidazolium chloride ([C_3mim]Cl) is the lowest as *ca.* 326 K (53°C) while 1-butyl-3-methylimidazolium chloride ([C_4mim]Cl) with the longest alkyl chain as *ca*. 341 K (68°C). Therefore, the effect of the length of the side chain of cation on T_m is not yet systematically understood.

In this study, the conventional differential scanning calorimetry (DSC) measurement was initially used to investigate T_m as a function of the composition of binary mixtures prepared from commercially available chemicals. However, the measurement sometimes failed, probably because a

small amount of moisture was absorbed during sample preparation, thereby hindering the coagulation of samples at low temperatures. The long measurement time for DSC also prevented efficient research progress. Therefore, more efficient methods for T_m investigation than DSC, *i.e.*, image processing and electrochemical impedance, were examined in this study. The eutectic composition of imidazolium chloride I.L. in binary and ternary systems was estimated.

2. Experimental

Three I.L. were used for experiments, as shown in **Fig. 1**, namely, 1-ethyl-3-methylimidazolium chloride ([C_2mim]Cl, >98%, Tokyo Chemical Industry, T_m = 352–358 K), 1-methyl-3-propylimidazolium chloride ([C_3mim]Cl, >98%, *ibid*, T_m = 325–328 K), and 1-butyl-3-methylimidazolium chloride ([C_4mim]Cl, >98%, *ibid*, T_m = 336–344 K). They were vacuum-dried in the liquid phase at 100°C for 12 h before experiments and sampled at defined composition with a total weight of *ca*. 5 g in a sample vial for video imaging experiments, and the temperature was reduced to coagulate the contents. In some cases, the liquid phase was not coagulated; thus, a small amount of salt solid was added to the vial to promote coagulation. Phase transition between solid and liquid phases was investigated using three methods, namely, DSC, video imaging, and electrochemical impedance. In the DSC measurement, *ca*. 5–10 mg mixture was stored in a sample case made of aluminum, placed in a chamber of DSC equipment (Hitachi High-Tech Co. model DSC 7000X), and the temperature was raised from 183 K (−90°C) to 393 K (120°C) with an increasing rate of 5 K min^{-1}. However, the measurement sometimes failed, probably because the absorption of a small amount of water during sample preparation prevented coagulation of I.L. below T_m. Thus, in this study, an alternative video imaging method was examined, as shown in **Fig. 2**. In this method, sample vials containing different compositions were placed in a temperature chamber, and the temperature was raised from 248 K (−25°C) to 368 K (95°C) with an increasing rate of 0.1 K min^{-1}. In this process, time-lapse images were taken at 10 s intervals using a USB endoscope camera (500M pixcel resolution, autofocus). A precise temperature sensor (Analog Devices, Inc., ADT7422) was placed in a chamber close to the vials. Considering the sample volume, heat capacitor, and heat transfer resistance of the vial glass wall, the temperature elevation rate was set to be sufficiently slow.

The melting start temperature (T_{ms}) and the melting end (complete) temperature (T_{me}) could be distinguished from the transition of time-lapse images. T_{ms} was judged by observing the flattening of the surface of solid I.L. T_{me} was the time when the content of the vial became completely transparent. However, T_{me} is also a function of heat transfer to and heat capacity of I.L. stored in a vial. Therefore, in this work, T_{ms} was regarded as T_m. One of the benefits of this method is that multiple samples with different compositions can be evaluated simultaneously. In this study, five samples were examined in a single run. Although T_{ms} and T_{me} obtained in this method contain uncertainty, it is expected that the eutectic composition X_e of the I.L. binary system is estimated. In some experiments, impedance spectra were also measured during temperature scanning to investigate the change in electric conductivity and determine whether they could be used as a criterion for the phase transition. Impedance spectra were measured once every 60 s using two Pt wire electrodes and an impedance analyzer (Ivium Technologies, model CompactStat) with a condition of f = 1–100 kHz and ΔE_{ac} = 10 mV.

3. Results and discussion

Figure 3 and **Table 1** show the resultant T_{ms} and T_{me} measured for the [C_2mim]Cl–[C_4mim]Cl binary system obtained using the video imaging method as a function of the molar fraction of [C_4mim]Cl, $X_{[C_4mim]Cl}$. T_{ms} and T_{me} contain some errors due to the ambiguity in determining the initiation and termination of phase transition (melting) from a video image. Therefore, T_{ms} and T_{me} at each $X_{[C_4mim]Cl}$ were speculated as regression curves of the dashed line shown in Fig. 3. The lowest T_{ms} = *ca*. 319 K was observed at the composition $X_{[C_4mim]Cl}$ = 0.45, which was close to the eutectic temperature (T_e) = 315 K at the eutectic composition of $X_{[C4mim]Cl}$ = 0.49 reported by M. Kick et al. [5] In the figure, DSC results are also shown on the left side, where the dependence of heat flow on the temperature at three $X_{[C_4mim]Cl}$ is presented. The endothermic peaks of three DSC curves were observed in the temperature range close to T_{ms} obtained in the video imaging method. T_{ms} tended to be higher than the peak temperature of the DSC measurement. The difference in T_{ms} and the DSC peak temperature originated from their methodologies. In the video imaging method, the surface melting of I.L. became apparent after the melting had progressed to some extent. On the other hand, in the DSC

measurement, the onset temperature of a peak was considerably lower than the peak temperature due to the preceding phase transition in the solid phase or gradual solid/liquid phase transition.

Figure 4 and **Table 1** show the result of the $[C_2mim]Cl$–$[C_3mim]Cl$ binary system. T_e = *ca.* 311 K was observed at the eutectic composition $X_{[C_3mim]Cl}$ = *ca.* 0.6. This is the lowest T_e among the three binary systems. **Figure 5** and **Table 1** show the results of the $[C_3mim]Cl$–$[C_4mim]Cl$ binary system, in which T_e = *ca.* 322 K was observed at $X_{[C_4mim]Cl}$ = *ca.* 0.5. The eutectic composition X_e and temperature of these two binary systems have not yet been reported. The T_m of $[C_3mim]C_l$ is the lowest among the three I.L. used in this study even though the length of the alkyl side chain is in the order of $[C_4mim]^+$ > $[C_3mim]^+$ > $[C_2mim]^+$. The low T_m of $[C_3mim]Cl$ is probably caused by the unstable solid phase packing of $[C_3mim]Cl$. This solid structure is stabilized (or moderated) by mixing with [C4mim]Cl, resulting in the clear phase transition at $X_{[C_4mim]Cl}$ = *ca.* 0.08 in the T_m–$X_{[C_4mim]Cl}$ curve of the $[C_3mim]Cl$–$[C_4mim]Cl$ binary system, as shown in **Fig. 5**. On the other hand, this stabilization effect by mixing with $[C_2mim]Cl$ to $[C_3mim]Cl$ is continuous, as shown in **Fig. 4**.

As shown in **Figs. 3–5**, the lowest T_e among the three binary systems was obtained in the $[C_2mim]Cl$–$[C_3mim]Cl$ mixture. As seen in these results, the X_e of a mixed system can be efficiently estimated using the video imaging method even though the T_e and X_e are not so accurate. T_{ms} obtained for $[C_2mim]Cl$, $[C_4mim]Cl$, and $[C_3mim]Cl$ at their molar fraction 1 in **Figs. 3–5** were not identical, thus containing some error in the order of a few Kelvin. **Table 2** lists the T_{ms} and the T_{me} for the three I.L. The averaged values of Tms of three I.L. in the table are the plausible values as the melting point. **Table 3** summarizes the T_e and X_e for the three binary systems.

The X_e of the three binary systems is close to the central composition of two I.L., indicating that lowering T_m is related to the entropy effect [1]. Thus, the same situation is expected for a ternary $[C_2mim]Cl$–$[C_3mim]Cl$–$[C_4mim]Cl$ system. Therefore, the T_{ms} and T_{me} of an $[C_2mim]Cl$–$[C_3mim]Cl$–$[C_4mim]Cl$ ternary system with a limited composition were investigated, as listed in **Table 4**. The three-component phase diagram is estimated from the binary diagrams (**Figs. 3–5**) and the data of the ternary system (**Table 4**), as shown in **Fig. 6**. Although the entire compositional area in the phase diagram of the ternary system was not evaluated due to the high experimental cost, it seems reasonable that the lowest T_{ms} was located around the equimolar composition of the ternary system. This is

because the entropy of the mixed system in the liquid phase is maximized at the equimolar condition, thereby lowering the free energy [2]. T_{ms} dropped to *ca.* 300 K, approximately 10 K lower than the T_e of the $[C_2mim]Cl$–$[C_3mim]Cl$ binary system shown in **Fig. 4**.

As seen in the results above, the melting point of coagulated I.L. estimated from the image analysis is not precise. On the other hand, an impedance measurement has been used to investigate the electric properties of I.L. [9-16] For example, the temperature dependence of the conductivity of the I.L. in the solid phase was proposed to follow the Vogel–Tammann–Fulcher (VTF) equation describing the temperature dependence of the relaxation time in a medium [13,14,16]. The electric conductivity of I.L. also drastically changes from a low conductive solid phase to a highly conductive liquid phase [9,10]. Therefore, it seems reasonable that the impedance technique is used to judge the criteria of the phase transition. In this study, the time transition of the impedance spectra of the $[C_2mim]Cl$ sample during temperature scanning was measured using two Pt wire electrodes to clarify the applicability of the impedance method to phase transition analysis. A precise temperature sensor was attached to a sidewall of a vial to evaluate the exothermic and endothermic processes. **Figure 7** shows the time transition of T and the time derivative of temperature (dT/dt) during upward and downward temperature scanning. In the upward scanning, any noticeable change in dT/dt curve was not observed in the temperature range (i) shown in **Fig. 3** around T_{ms} and T_{me} because the endothermic phase transition proceeded slowly in this temperature range. On the other hand, a sharp spike was observed in the downward temperature scanning at *ca.* T = 302 K (ii) caused by the rapid exothermic coagulation of supercooled $[C_2mim]Cl$ liquid. This result shows that T_m cannot be determined during an increase in temperature from the temperature measurement in this experimental configuration.

Figure 8(a) and **(b)** shows impedance Bode diagrams of two Pt wire electrodes in $[C_2mim]Cl$ I.L. during upward and downward temperature scanning, respectively. The lowest frequency of the spectra was limited to 1 Hz to reduce the measurement time to follow the rapid phase transition. As shown in **Fig. 8(a)**, the Bode plot reveals a resistive response at R = *ca.* 400 kΩ in a wide frequency range less than f < 10 kHz at T = 283 K. This high resistance corresponds to the low ionic conductance of $[C_2mim]Cl$ in a solid phase. The R decreased as the temperature (T) increased and revealed the capacitive response in a low-frequency range at T > 340 K. The appearance of this

capacitance is attributed to the evolution of the liquid phase on the electrodes, similar to the electric double layer in an aqueous electrolyte solution. On the other hand, the Bode plot during a decrease in temperature shows the decreasing impedance with decreasing T, as shown in **Fig. 8(b)**. Around T = 303 K, a discontinuous transition of impedance was observed corresponding to the dT/dt spike (ii) shown in **Fig. 7**. The abnormal behavior of phase at T = 303 K was caused by the rapid transition during frequency scanning in the impedance measurement. Impedance Z increased with decreasing T, corresponding to the ratio of solid/liquid phases.

The conductivity of a medium corresponds to the inversed resistance R^{-1}. The R^{-1} calculated from $|Z|$ and phase angle θ at f = 1 kHz as $R^{-1} = 1/(|Z| \cos\theta)$ was plotted against T during upward and downward temperature scanning in **Fig. 9**. Similar plots were also obtained at different frequencies of f = 100 Hz and 10 kHz. The R^{-1} shows a continuous increase during an increase in temperature. The R^{-1} in a log scale increases linearly with T at $T < ca.$ 340 K, indicating that the conductivity of [C_2mim]Cl in the solid phase follows the VTF relationship, an empirical formula describing the temperature dependence of the relaxation time in a medium [9,13,14,16]:

$$\sigma = Aexp\left(\frac{-C}{T-T_g}\right)$$

where σ represents the electric conductivity, A and C are constant, and T_g represents a glass transition point. This equation has been used for the interpretation of the ionic conductivity of I.L. [10,13] At $T > ca.$ 340 K, a slope of log R^{-1}-T curve increases, and a liquid phase begins to appear at the top of the solid phase in video image b at $T > T_{ms}$. A slope of log R^{-1}-T curve dropped at $T > T_{me}$, where most of the solid melted (image c). Therefore, the entire conductivity σ of the sample between T_{ms} and T_{me} is a summation of the conductivities of the solid phase (σ_S) and liquid phase (σ_L) at their composition X_S and X_L as $\sigma = X_S\sigma_S + X_L\sigma_L$.

During decreasing temperature, R^{-1} changed discontinuously at the phase transition (ii) due to rapid exothermal coagulation in supercooled conditions. The video images (d)–(f) show that the coagulation proceeded rapidly (60 s interval per each image), and R^{-1} dropped rapidly accompanying the coagulation. Such different phase transition temperature in the temperature increase and decrease has been generally observed in the DSC measurement [1,5] and impedance measurement.[10] This

result confirms that the electric conductance measurement using an impedance method is useful to investigate the phase transition process.

As discussed above, the increasing rate of R^{-1} against T during increasing temperature is reflected by the temperature dependence of σ_S and σ_L, and the composition of the solid and liquid phases (X_S, X_L). Therefore, the gradient dR^{-1}/dT during the phase transition is expected to change with changing the Xs/X_L ratio. In **Fig. 10**, R^{-1} and (dR^{-1}/dT) during increasing temperature were plotted against T. The DSC signal (thermal flow) was also plotted for comparison. A peak of the (dR^{-1}/dT) curve was observed between T_{ms} and T_{me}, and the shape of the peak is similar to the DSC peak even though the temperature range of the two peaks was different. As discussed previously, the discrepancy may originate from the difference in the sample volume or the measurement condition. When the melting proceeded, melt at the top of the sample was observed at the location pointed by the arrow in the picture (b). At the end of the melting process, slight muddiness, which was a suspension of small floating solids, remained at the location pointed by the arrow in the picture (c). The sample, then, became completely transparent at $T > T_{me}$. As seen in this result, the impedance of I.L. is significantly influenced by the condition and composition of the liquid/solid phases. Therefore, the impedance method is useful for determining the T_m of I.L.

A thin glass cell with an internal dimension of 2 mm in thickness and 20 mm in width was used for impedance measurement to reduce the I.L. volume, as shown in **Fig. 11**. However, the results indicate that the liquid phase always existed at the top of the sample, even at the low-T range. The formation of the liquid phase was probably caused by the absorption of water even though sample transfer was performed in a glove box filled with dried N_2 gas. Therefore, R^{-1} during increasing temperature was considerably larger than that shown in **Fig. 9** due to the existence of the high conductive liquid phase, and the transition of R^{-1} at the melting point was not so obvious. However, the (dR^{-1}/dT) curve shows a clear peak at T, almost the same as that shown in **Fig. 10**. During decreasing temperature, a transition of R^{-1} at the coagulation temperature was also small because of little exotherm from a small amount of sample, and I.L. did not completely solidify at the lower temperature. In conclusion, the differential (dR^{-1}/dT)-T curve measurement is useful in determining T_m, even if only a part of the I.L. showed the solid/liquid phase transition.

4. Conclusions

The eutectic temperature T_e and composition X_e of a binary system composed of three I.L., *i.e.*, [C_2mim]Cl, [C_3mim]Cl, and [C_4mim]Cl, were estimated using a video imaging method, in which the formation of the liquid phase on the solid phase was assessed from the time-lapse images of I.L. at a given composition stored in a vial taken during temperature scanning in a chamber. The advantage of this method is that multiple samples (five samples in this study) were measured simultaneously, significantly reducing the experimental time. On the other hand, the disadvantages of this method are the less accurate determination of the melting point and significant usage of high-cost chemicals compared with the DSC method. For example, a measurement error of several degrees Celsius could remain in determining the melting point. The T_e and X_e of [C_2mim]Cl–[C_3mim]Cl, [C_2mim]Cl–[C_4mim]Cl, and [C_3mim]Cl–[C_4mim]Cl binary systems were roughly estimated. Furthermore, the T_e of the [C_2mim]Cl–[C_3mim]Cl–[C_4mim]Cl ternary system with almost equimolar compositions was estimated to be lower than that of the binary systems. The transition of the electrochemical impedance of [C_2mim]Cl I.L. was also measured using two Pt wire electrodes as a function of temperature. The differential inversed resistance curve (dR^{-1}/dT)-T shows a clear peak corresponding to the phase transition from a low conductive solid phase to a highly conductive liquid phase. This peak temperature was comparable with the T_m obtained in the video imaging method and differed from the T_m obtained in the DSC measurement. In conclusion, the impedance method is useful for determining ionic liquids' melting points.

Reference

[1] T. D. J. Dunstan, J. Caja, *ECS Transactions*, **3** (2007) 21-32.

[2] H. Niedermeyer, J. P. Hallett, I. J. Villar-Garcia, P. A. Huntand, T. Welton, *Chemical Society Review,* **41** (2012) 7780-7802.

[3] G. Chatel, J. F. B. Pereira, V. Debbeti, H. Wang, R. D. Rogers, *Green Chemistry*, **16** (2014) 2051-2083.

[4] M. Smiglak, N. J. Bridges, M. Dilip, R. D. Rogers, *Chemistry. A European Journal,* **14** (2008) 11314-11319.

[5] M. Kick, P. Keil, A. König, *Fluid Phase Equilibria*, **338** (2013) 172-178.

[6] O. Stolarska, A. Soto, H. Rodríguezcand, M. Smiglak, *RSC Advances*, **5** (2015) 22178-22187.

[7] S. K. Das, D. Majhi, P. Kumar Sahu, M. Sarkar: *RSC Advances* **5** (2015) 41585-41594.

[8] M. Ebrahimi, F. Moosavi: *Journal of Molecular Liquids* **250** (2018) 121-130.

[9] J. Vila, C. Franjo, J.M. Pico, L.M. Varela, O. Cabeza, *Portugaliae Electrochimica Acta,* **25** (2007) 163-172.

[10] J. Vila, B. Fernández-Castro, E. Rilo, J. Carrete, M. Domínguez-Pérez, J. R. Rodríguez, M. García, L. M. Varela, O. Cabeza, *Fluid Phase Equilibria* **320** (2012) 1-10.

[11] O. Yamamuro, Y. Minamimoto, Y. Inamura, S. Hayashi, H. Hamaguchi, *Chemical Physics Letters*, **423** (2006) 371-375.

[12] J. Vila, L. M. Varela, O. Cabeza, *Electrochimica Acta* **52** (2007) 7413-7417.

[13] J. Vila, P. Ginés, J. M. Pico, C. Franjo, E. Jiménez, L. M. Varela, O. Cabeza, *Fluid Phase Equilibria* **242** (2006) 141-146.

[14] S. Papović, S. Gadžurić, M. Bešter-Rogač, M. Vraneš, *The Journal of Chemical Thermodynamics* **102** (2016) 367-377.

[15] A. Šantić, W. Wrobel, M. Mutke, R. D. Banhatti K. Funke, *Phys. Chem. Chem. Phys*., **11** (2009) 5930-5934.

[16] J. Leys, M. Wübbenhorst, C. P. Menon, R. Rajesh, J. Thoen, C. Glorieux, P. Nockemann, B. Thijs, K. Binnemans, S. Longuemart, *The Journal of Chemical Physics* **128** (2008) 064509.

Table 1. The melting start (T_{ms}) and complete (T_{me}) temperature of coagulated binary ionic liquids as a function of composition evaluated by the imaging method.

[C_2mim]Cl-[C_4mim]Cl (Fig.3)			[C_2mim]Cl-[C_3mim]Cl (Fig.4)			[C_3mim]Cl-[C_4mim]Cl (Fig.5)		
$X_{[C_4mim]Cl}$	T_{ms} / K	T_{me} / K	$X_{[C_3mim]Cl}$	T_{ms} / K	T_{me} / K	$X_{[C_4mim]Cl}$	T_{ms} / K	T_{me} / K
0.00	357.9	365.2	0.00	352.5	363.1	0.00	327.6	330.4
0.09	352.0	356.1	0.10	345.9	356.6	0.00	325.6	330.0
0.18	339.2	349.8	0.19	335.2	345.3	0.00	327.5	329.1
0.27	331.6	341.6	0.28	329.2	345.0	0.06	324.1	328.2
0.36	320.0	336.8	0.37	320.1	335.0	0.09	334.5	339.0
0.46	319.6	326.8	0.40	318.4	330.7	0.16	330.2	335.8
0.52	320.2	323.8	0.42	317.4	329.2	0.19	328.8	333.7
0.56	321.9	325.2	0.44	315.4	328.0	0.28	325.2	330.2
0.65	325.0	330.5	0.45	314.3	327.0	0.32	327.0	329.7
0.88	337.8	340.4	0.49	311.3	324.4	0.36	325.9	328.2
1.00	336.5	342.4	0.50	313.7	323.1	0.40	321.9	327.3
			0.51	313.0	323.1	0.48	321.7	326.6
			0.54	311.5	323.3	0.53	321.4	329.6
			0.56	311.5	318.0	0.55	323.9	329.3
			0.57	311.6	318.7	0.58	325.0	330.2
			0.61	311.2	317.1	0.61	325.8	329.8
			0.62	310.5	316.9	0.65	326.2	331.0
			0.68	314.5	317.9	0.69	328.4	333.2
			0.78	315.5	324.3	0.79	333.8	337.3
			0.88	321.5	326.1	0.90	335.2	341.6
			1.00	327.5	329.1	1.00	343.7	347.8

Table 2. The melting start (T_{ms}) and complete (T_{me}) temperature of coagulated ionic liquids evaluated by the imaging method.

	T_{ms} / K	T_{me} / K	Source
[C_2mim]Cl	357	364	Fig. 3
	353	363	Fig. 4
	355	363.5	Average
[C_3mim]Cl	327	329	Fig. 4
	326.5	329	Fig. 5
	326.8	329	Average
[C_4mim]Cl	339	343	Fig. 3
	341	347	Fig. 5
	340	345	Average

Table 3. Eutectic composition (E.C.) and melting point estimated for [C_2mim]Cl–[C_4mim]Cl, [C_2mim]Cl–[C_3mim]Cl, and [C_3mim]Cl–[C_4mim]Cl binary systems.

Mixed system	T_e / K	$T_{e(Ref.5)}$ / K	X_e	$X_{e(Ref.5)}$
[C_2mim]Cl–[C_4mim]Cl	319	315	$X_B = 0.45$	0.49
[C_2mim]Cl–[C_3mim]Cl	311	-	$X_P = 0.6$	-
[C_3mim]Cl–[C_4mim]Cl	322	-	$X_B = 0.5$	-

Table 4. Melting point estimated for [C_2mim]Cl–[C_4mim]Cl–[C_3mim]Cl ternary systems.

[C_2mim]Cl : [C_4mim]Cl : [C_3mim]Cl	T_{ms} / K	T_{me} / K
0.230 : 0.408 : 0.362	293	315
0.335 : 0.332 : 0.331	299	308
0.328 : 0.329 : 0.344	299	311
0.373 : 0.329 : 0.298	302	308

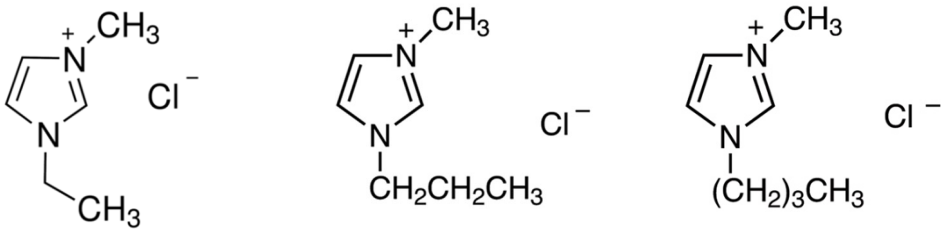

[C_2mim]Cl [C_3mim]Cl [C_4mim]Cl

Fig. 1. Three ionic liquids used in the present work. [C_2mim]Cl (1-ethyl-3-methylimidazolium chloride), [C_3mim]Cl (1-methyl-3-propylimidazolium chloride), and [C_4mim]Cl (1-butyl-3-methylimidazolium chloride).

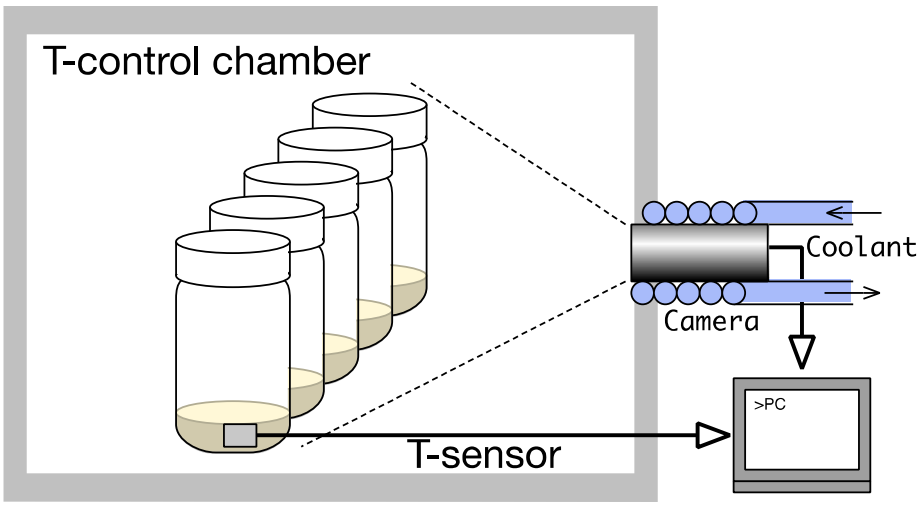

Fig. 2. Setup for video imaging method.

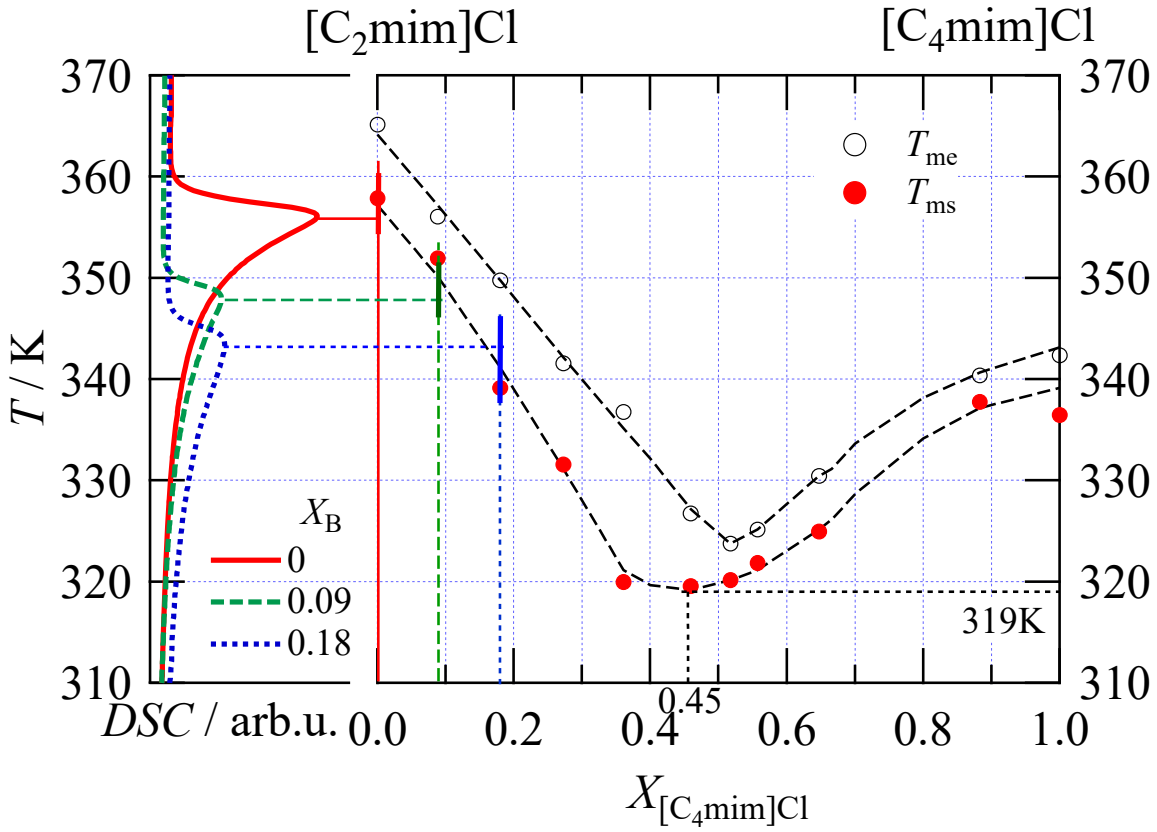

Fig. 3. Dependence of a melting start temperature (T_{ms}) and a melting end temperature (T_{me}) on a molecular fraction of [C4mim]Cl in a mixture of [C2mim]Cl and [C4mim]Cl, $X_{[C_4mim]Cl}$. The left side is a heat flow plot of DSC measurement for a mixture of [C2mim]Cl and [C4mim]Cl at three $X_{[C_4mim]Cl}$ values.

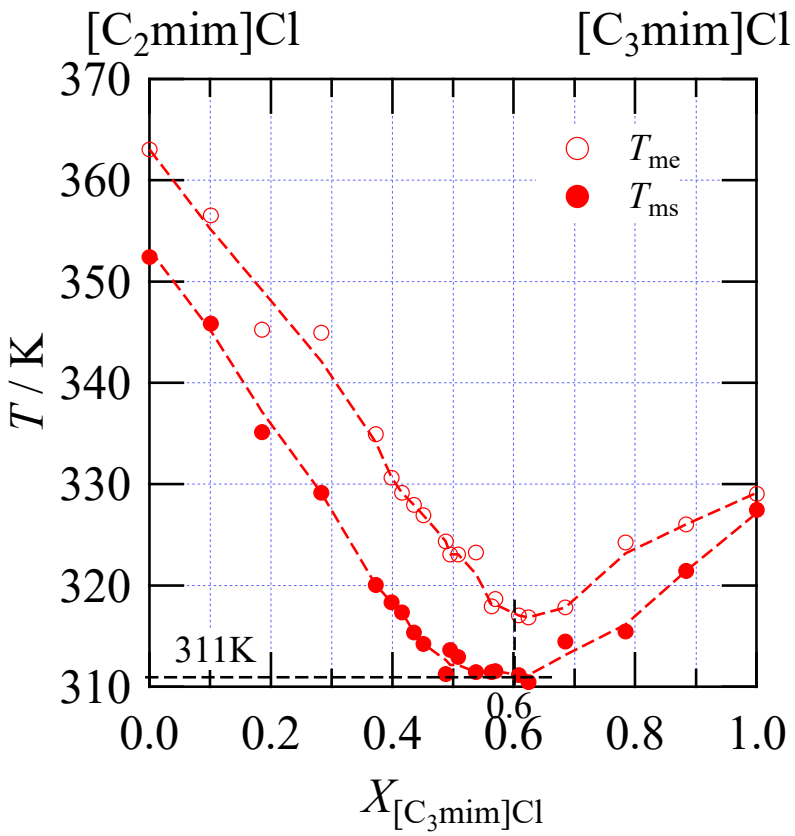

Fig. 4. Dependence of a melting start temperature (T_{ms}) and a melting end temperature (T_{me}) on a molecular fraction of [C3mim]Cl in a mixture of [C2mim]Cl and [C3mim]Cl, $X_{[C_3mim]Cl}$.

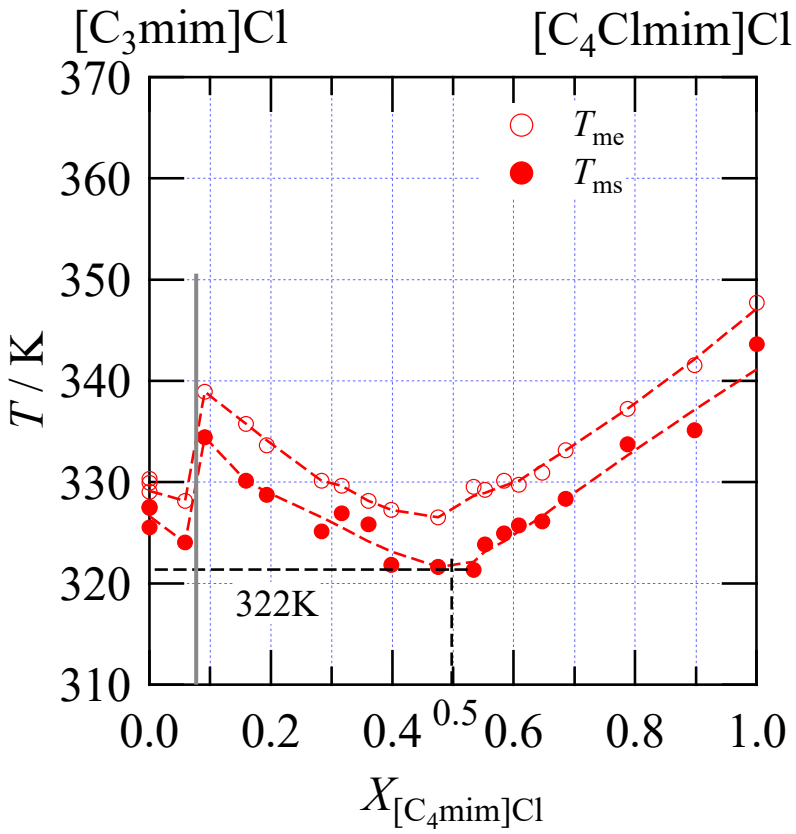

Fig. 5. Dependence of a melting start temperature (T_{ms}) and a melting end temperature (T_{me}) on a molecular fraction of [C_4mim]Cl in a mixture of [C_3mim]Cl and [C_4mim]Cl, $X_{[C_4mim]Cl}$.

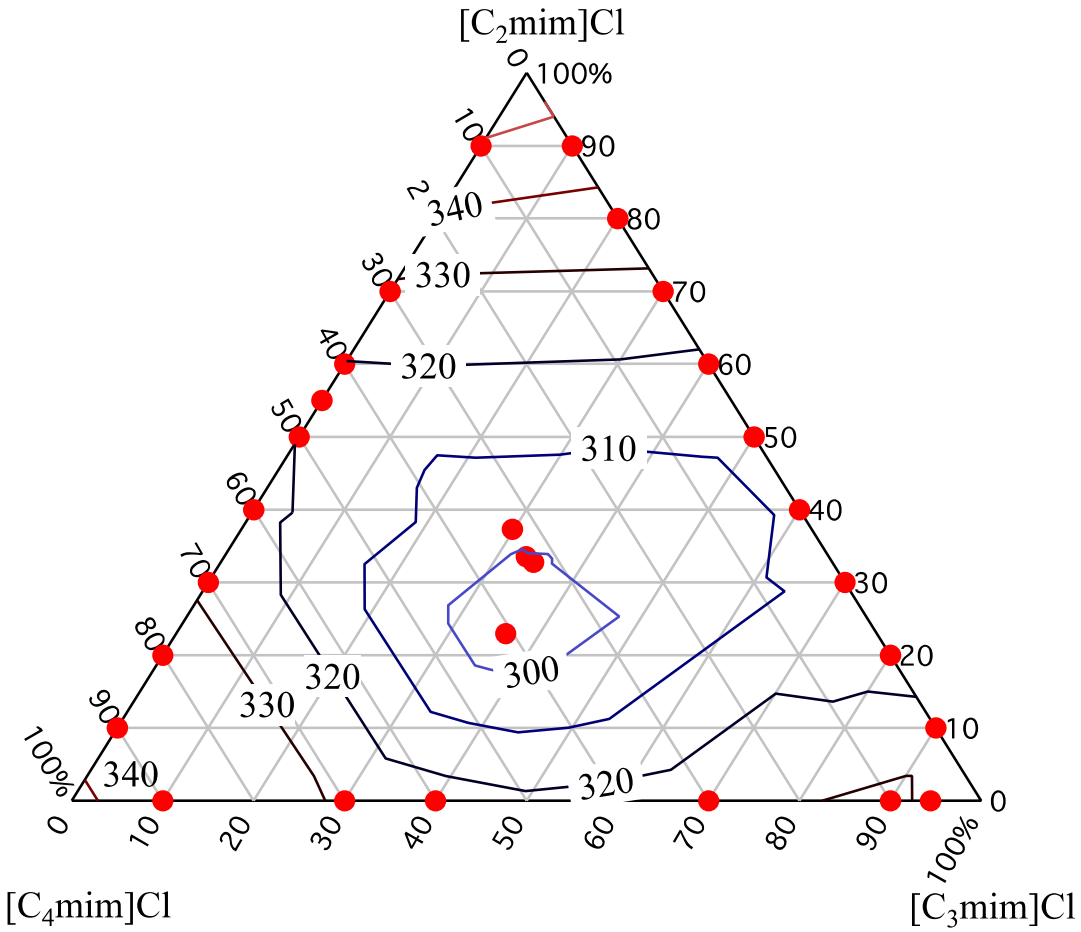

Fig. 6. Three-phase diagram roughly speculated from three binary diagrams shown in **Figs. 3–5** and limited ternary system presented in **Table 4**.

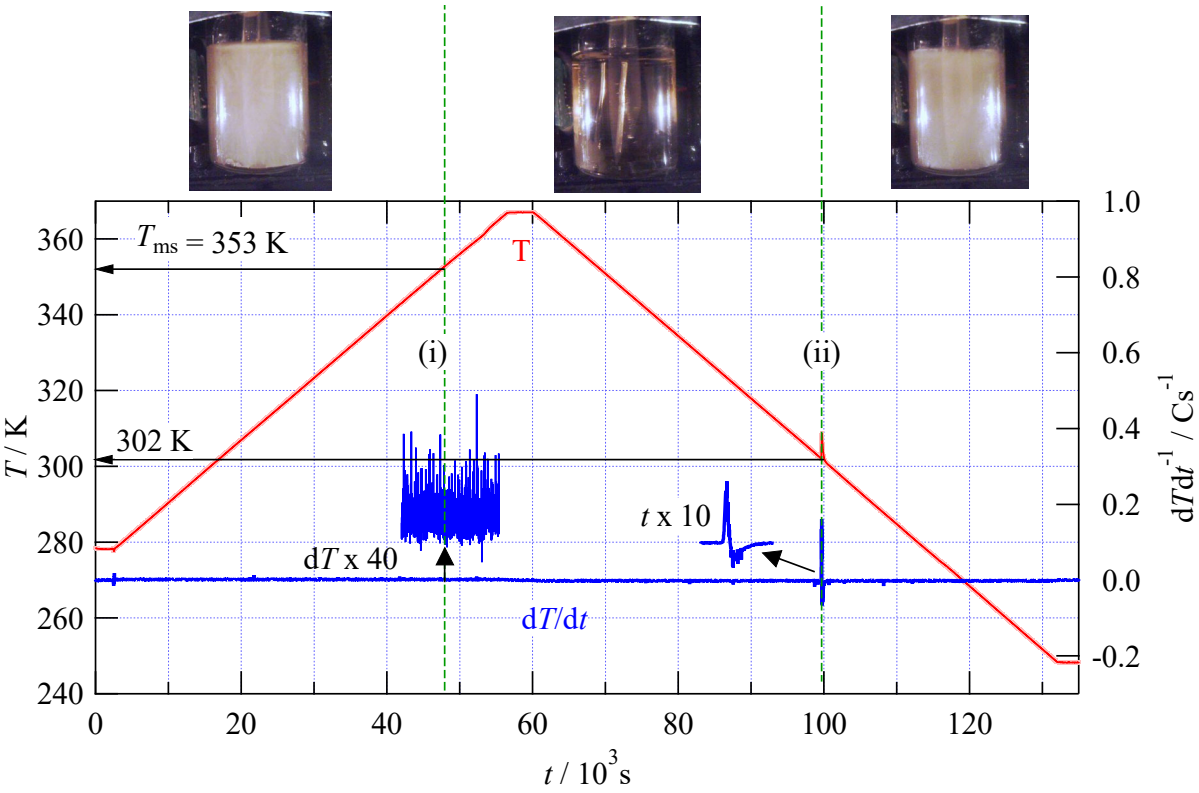

Fig. 7. Time transition of temperature and differential temperature during temperature scanning.

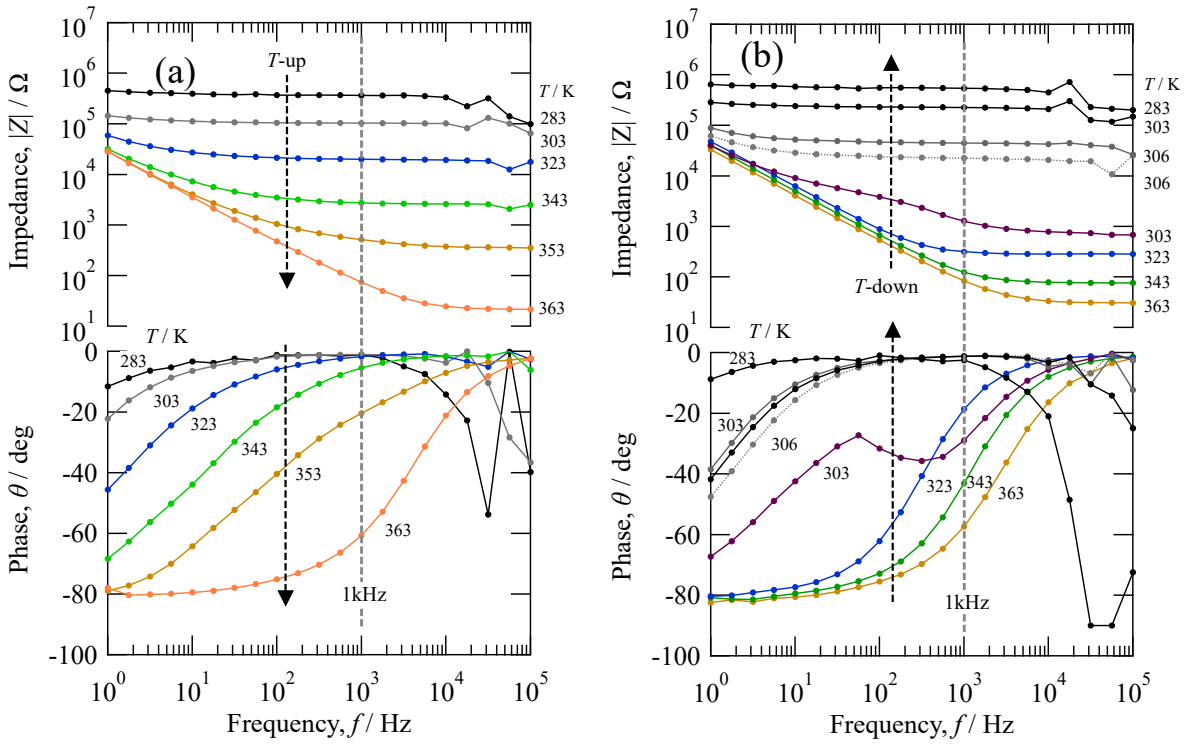

Fig. 8. Bode plot of two Pt electrodes immersed in [C_2mim]Cl ionic liquid as a function of temperature (increasing and decreasing).

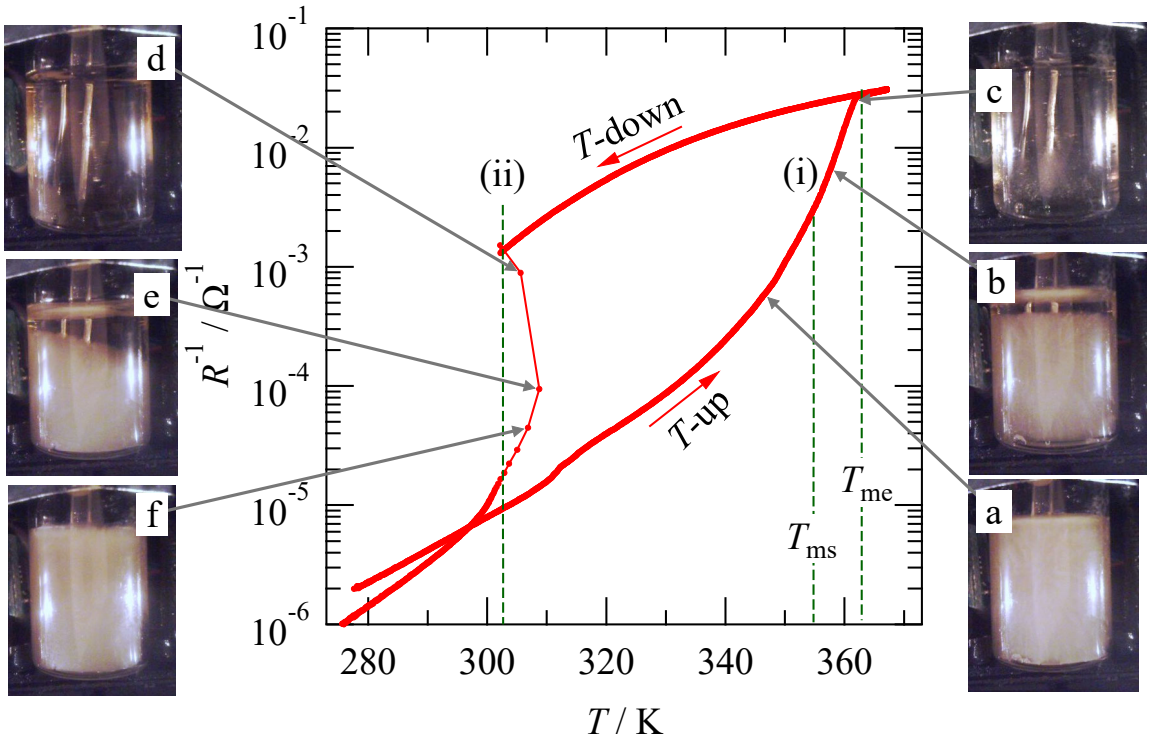

Fig. 9. Transition of reversal electric resistance R^{-1} of [C_2mim]Cl calculated from impedance at 1 kHz in the temperature scanning.

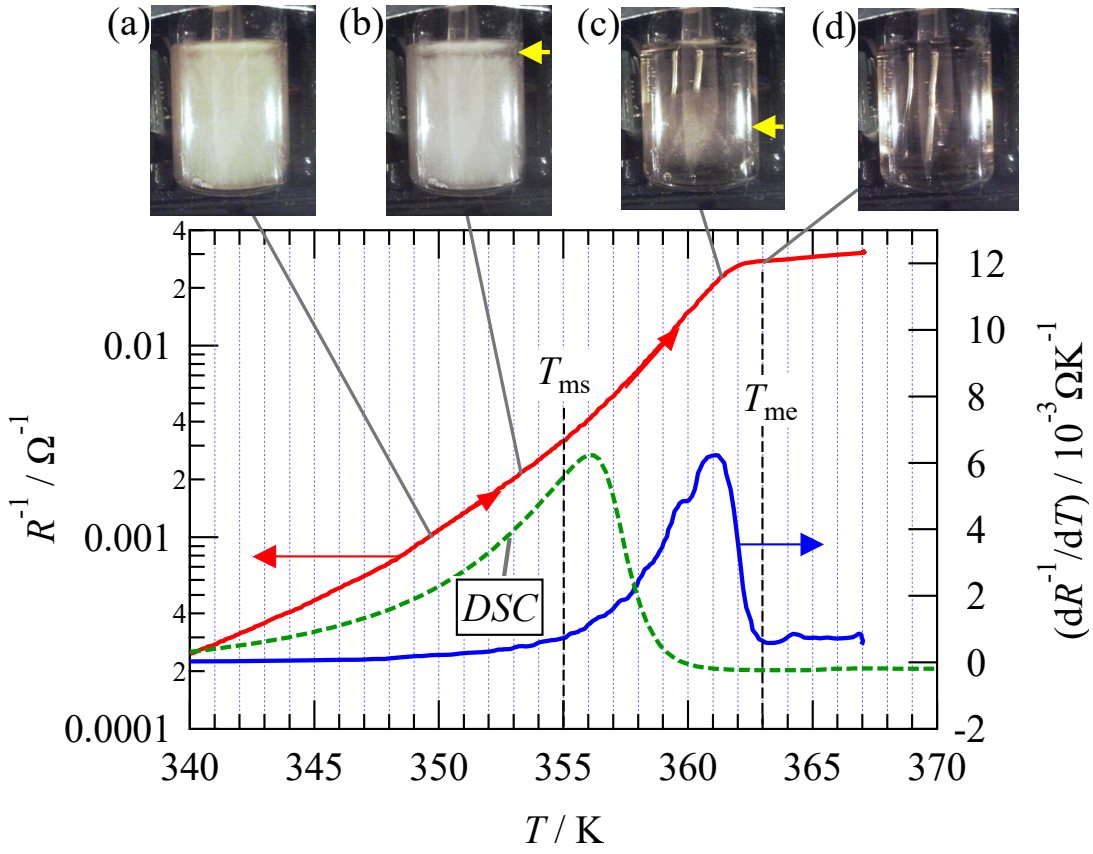

Fig. 10. Temperature dependence of reversal resistance R^{-1} and differential $dR^{-1}dT^{-1}$ of $[C_2mim]Cl$ during temperature elevation. The *DSC* signal in an arbitrary unit is also presented for comparison.

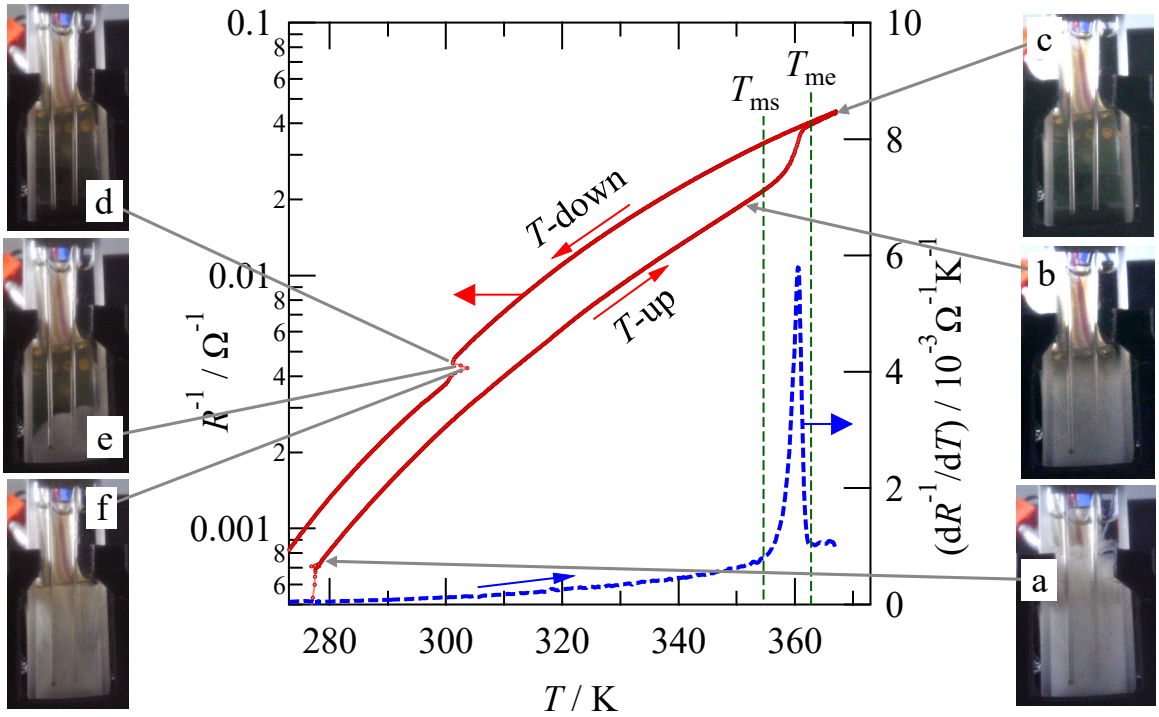

Fig. 11. Temperature dependence of reversal resistance R^{-1} and differential $dR^{-1}dT^{-1}$ of [C_2mim]Cl calculated from impedance data at 1 kHz during temperature elevation.